ON THE SPIN-DOWN OF AXP's AND SGR's AS PULSAR WHITE DWARFS

Diego Leonardo Cáceres Uribe.
In colaboration with: Jorge Rueda, Remo Ruffini
Kuantaky Boshkayev, Manuel Malheiro, Jaziel Coelho, Rafael Camargo

Tuesday 28th June 2016

Dipartimento di Fisica
Sapienza Università di Roma
Supernovae, Hypernova and Binary Driven Hypernovae - An Adriatic Workshop
International Center for Relativistic Astrophysics Network - Pescara
Italy

Contents

1 **Introduction** 3

2 **Rotation power in the white dwarf model** 5

3 **Radius from the optical emission** 9

4 **Magnetosphere of rotationally powered pulsars** 12

5 **Polar Cap Model** 15

5.1 Pulsar death-line or pair production threshold 15

5.2 Luminosity and temperature from bombardment of positrons 16

6 **Outer gap model** 19

7 **Conclusions** 23

1. Introduction

- Soft Gamma Ray Repeaters (SGRs) and Anomalous X-ray Pulsars (AXPs) are a class of compact objects that show some peculiar observational properties:

  – Rotational periods in the range $P \sim (2 - 12)$s. For ordinary pulsars, $P \sim (0.001 - 10)$s.

  – Spin-down rates $\dot{P} \sim (10^{-13}{-}10^{-10})$ larger than ordinary pulsars, $\dot{P} \sim 10^{-15}$.

  – Non detection of a binary companion.

  – If described as White Dwarf-like ordinary pulsars, $\dot{E}_{\rm rot} > L_{\rm X}$, (see Paczynski 1990 and Usov 1993)

  – Traditionally pulsars have been considered as rotating dipole in vacuum, so magnetic fields could be infered. But with recent simulations in axysimmetric (Contopoulos et. al. 2014) and non-axysimmetric (spitkovsky 2006) configurations, new spin-down formulas have been obtained

- The traditional formula for the spin-down of a 90 rotating vacuum dipole:

$$L(\theta)_{\text{vacuum}} \approx L_{\text{vacuum}}(90) = \frac{B^2 r^6 \Omega^4}{6c^3} \tag{1}$$

where B, r, Ω are the polar values of the magnetic field, the radius of the compact star and the star's angular velocity, respectively.

- Following Force-free Electrodynamics, Spitkovsky 2006 evolved numerically an oblique dipolar magnetosphere, obtaining a constant electromagnetic energy flux given by:

$$L_{\text{Spitkovsky}}(\theta) = \frac{B^2 r^6 \Omega^4}{4c^3}(1 + \sin^2\theta) \tag{2}$$

- Modifying some boundary conditions, Contopoulos et. al. 2014 obtained a new expression for the spin-down in the case of an axially symmetric pulsar:

$$L_{\text{Contopoulos}} = 0.82\frac{B^2 \Omega^4 r^6}{4c^3} \tag{3}$$

2. Rotation power in the white dwarf model

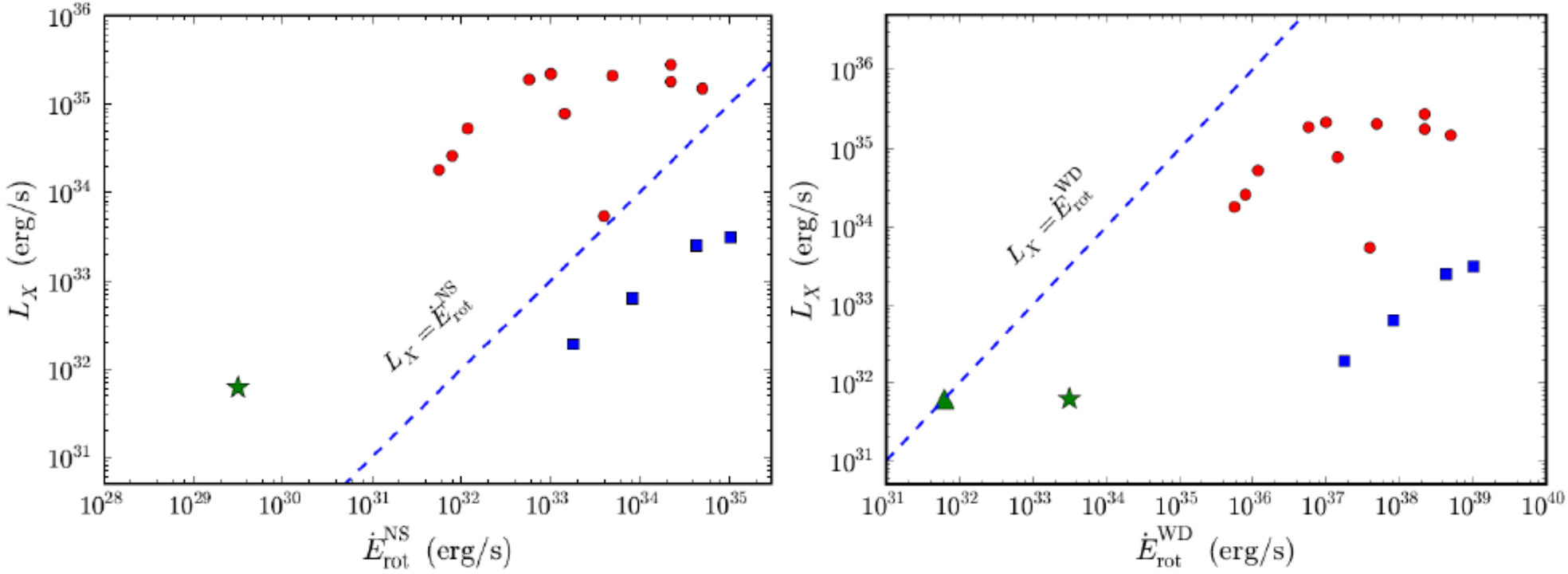

Figure 1. X-ray luminosity vs the loss of rotational energy $\dot{E}_{\rm rot}$ describing SGRs and AXPs as NS (left) and WDs (right). The green star and the green triangle correspond to SGR 0418+5729 using respectively the upper and lower limit of $\dot{P}$, $\dot{P} < 6.0 \times 10^{-15}$. The blue squares are the only four sources that satisfy $L_{\rm X} < \dot{E}_{\rm rot}$ when described as NSs. Taken from Malheiro et, al. 2012, (arXiv:1102.0653v7).

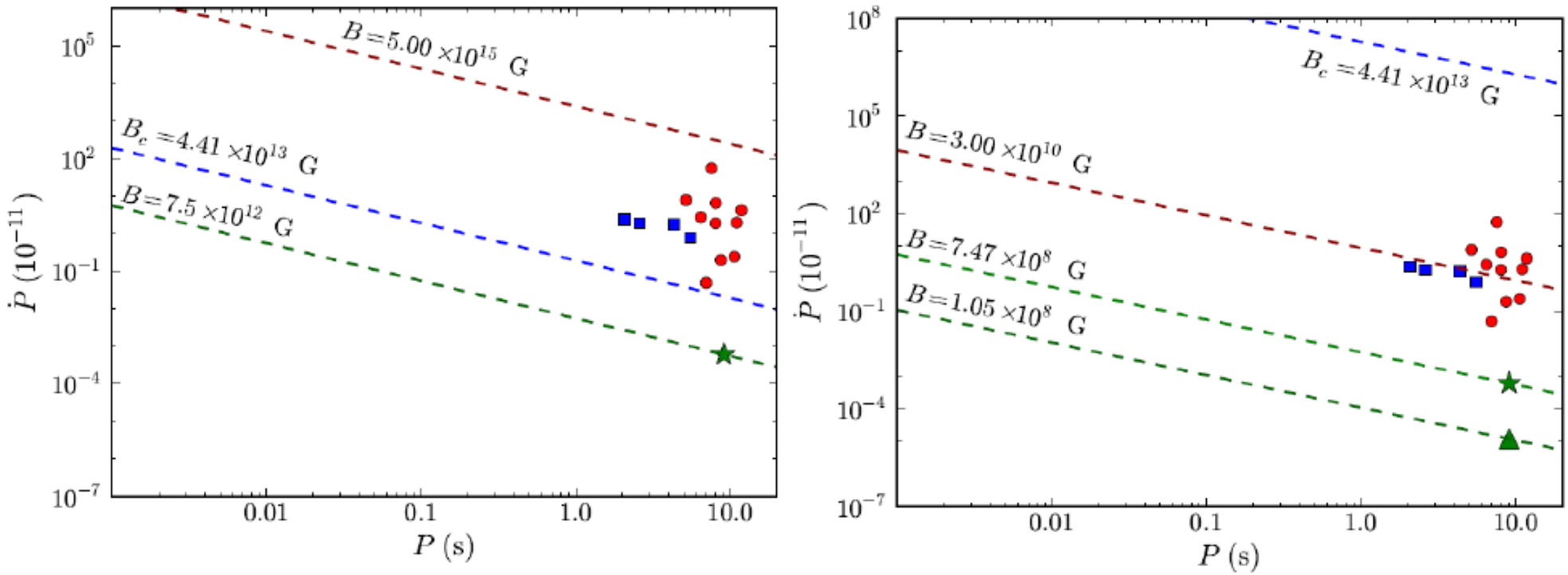

Figure 2. $\dot{P} - P$ diagram for all known SGRs and AXPs. The curves of constant magnetic field for neutron stars (left) and white dwarfs (right) are shown. The blue dashed line corresponds to the critical magnetic field $B_{\rm c} = m_{\rm e}^2 c^3/(e\hbar)$. The green star corresponds to SGR 0418+5729 using the upper limit of $\dot{P}$, $\dot{P} < 6.0 \times 10^{-15}$. The blue squares are the only four sources that satisfy $L_{\rm X} < \dot{E}_{\rm rot}$ when described as rotation powered NSs. Taken from Malheiro et, al. 2012, (arXiv:1102.0653v7).

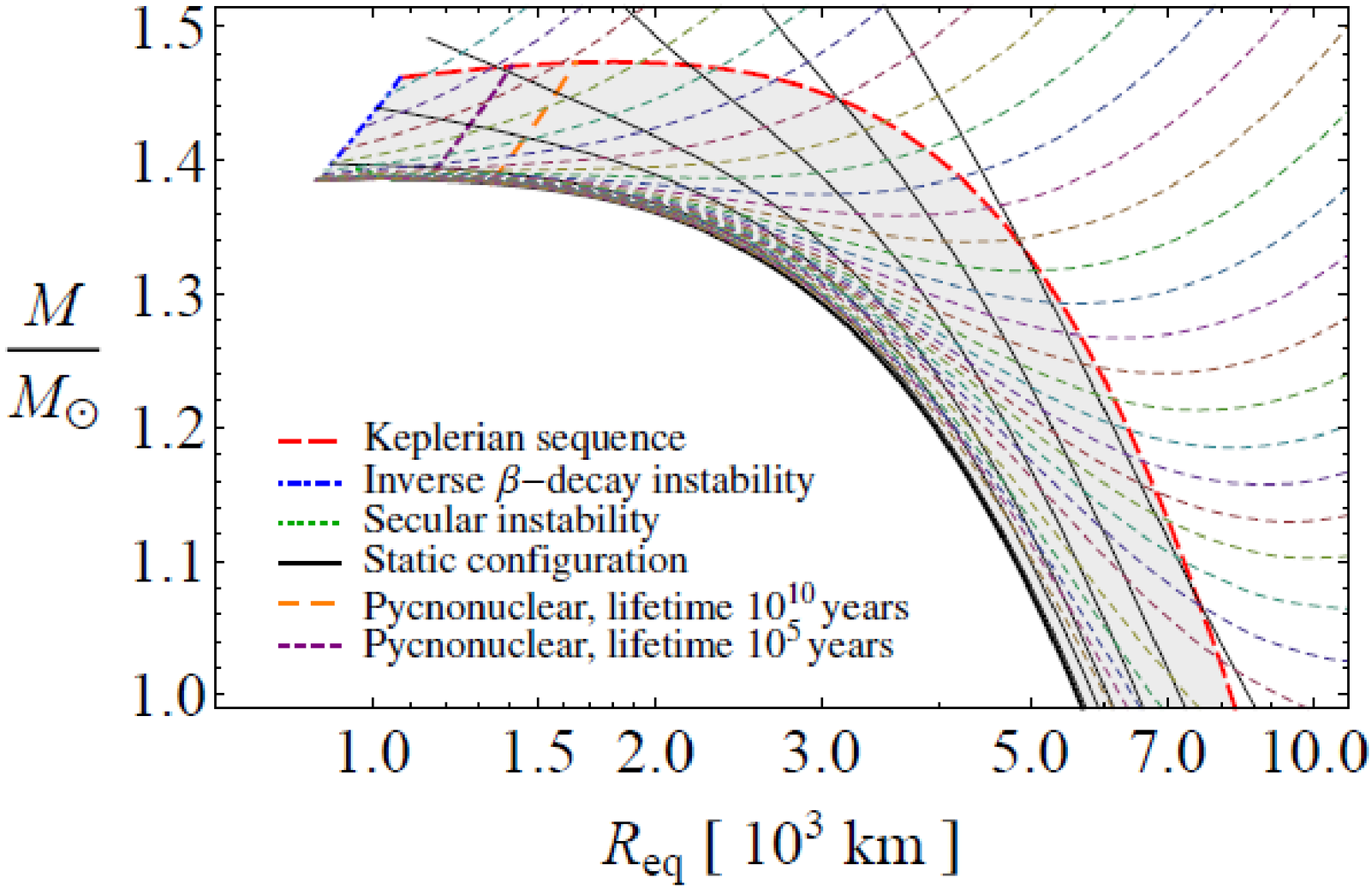

Figure 3. Mass vs equatorial radius of rotating ^{12}C WDs. The color thin dashed line correspond to P =constant sequence. The gray-shaded region is the stability region of rotating white dwarfs. Taken from Boshkayev et. al., A&A 555:A151 (2013)

The upper limit on the polar magnetic field for the vacuum case is:

$$B = \sqrt{\frac{3c^3}{2\pi^2}\frac{I}{\overline{R}^6}P\dot{P}} \tag{4}$$

where $\overline{R} = (2R_{\rm eq} + R_{\rm p})/3$ is the mean radius, with $R_{\rm eq}$ and $R_{\rm p}$ the equatorial and polar radius of the star.

Source	$M_{\rm min}$	$M_{\rm max}$	$\overline{R}_{\rm max}$	$\overline{R}_{\rm min}$	$B_{\rm min}$	$B_{\rm max}$
1E2259+586	1.24	1.39	1.04	5.34	1.27×10^8G	2.76×10^9G
SGR0418+5729	1.15	1.39	1.05	6.18	1.19×10^7G	3.49×10^8G

Table 1. Bounds for the mass M (in units of $M_\odot$), mean R radius (in units of 10^8cm) and upper limit of the magnetic field (obtained using equation (4)) for two sources. Values obtained from Boshkayev et. al., A&A 555:A151 (2013).

3. Radius from the optical emission

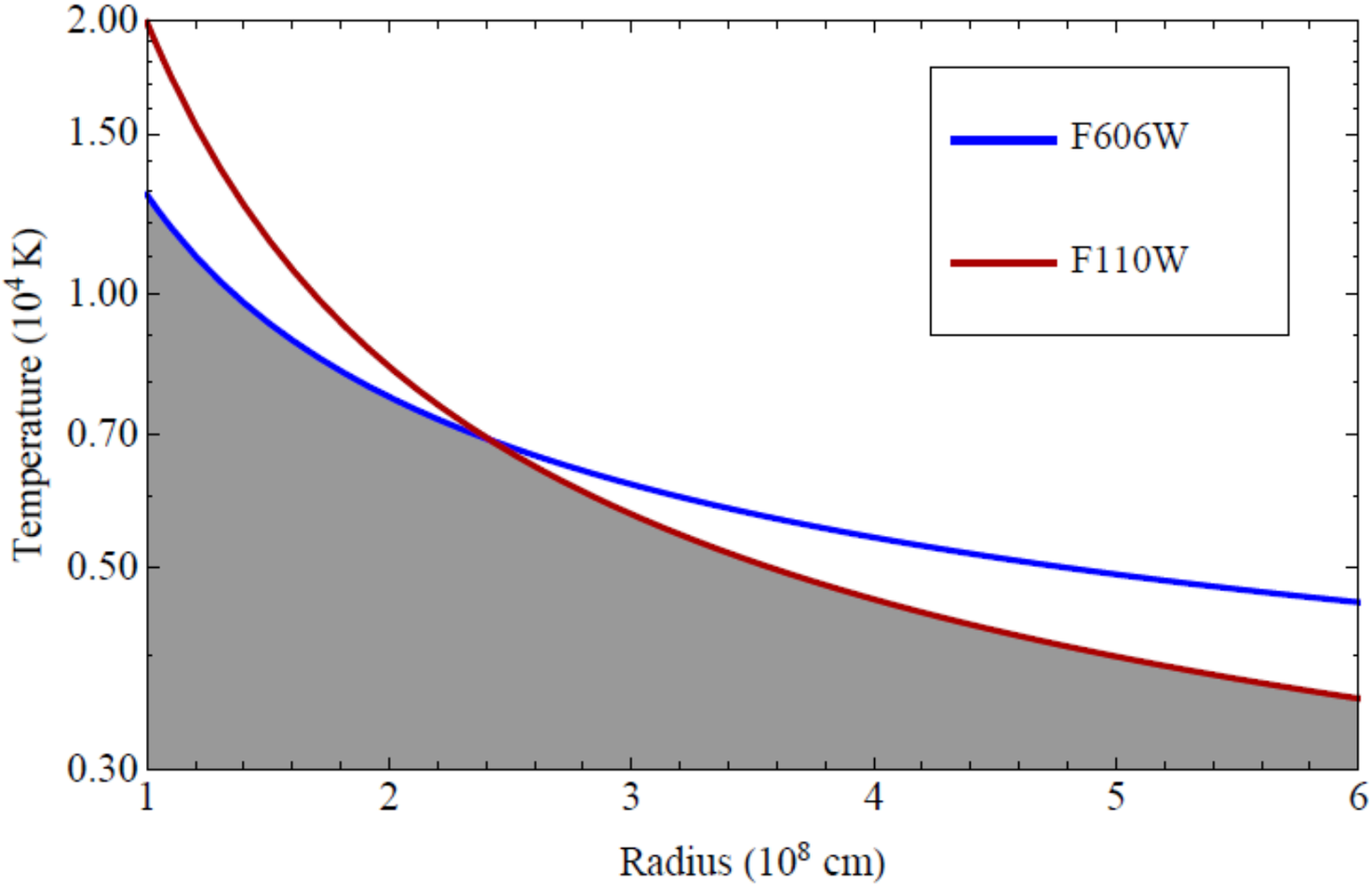

Figure 4. Temperature-Radius constraint for observed SGR 0418+5729 with the two wide filters F606W and F110W of the Hubble space telescope. Durant et. al. ApJ 747, 77 (2011) derived the upper limits of the apparent magnitude, $m_{\mathrm{F606W}} > 28.6$ and $m_{\mathrm{F606W}} > 27.4$. Taken from Boshkayev et. al. A&A 555:A151 (2013).

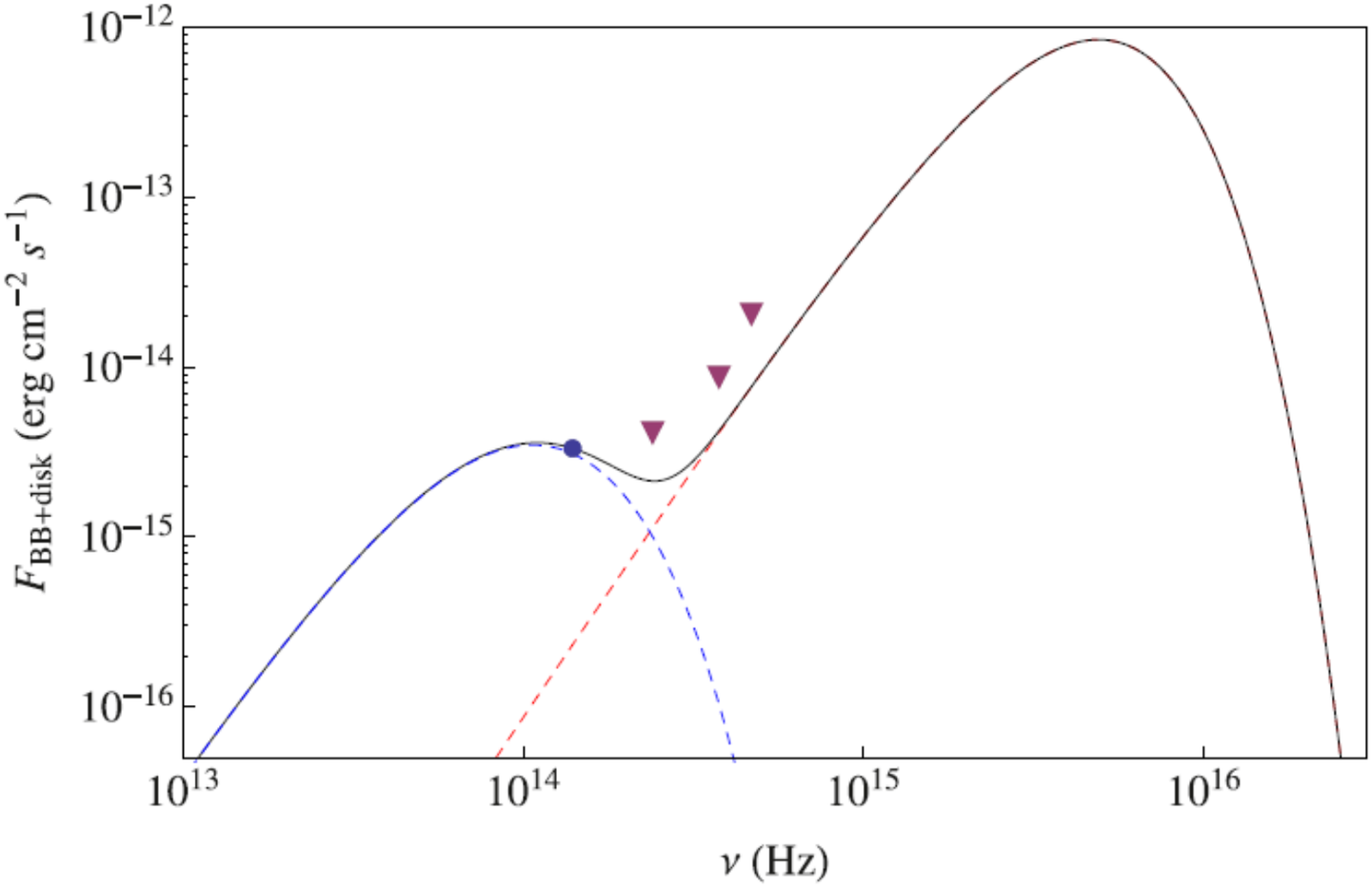

Figure 5. Observed and fitted spectrum of 1E2259+5726. The filled circle is the observed flux in the K_s band (near-IR counterpart) and the triangles are the upper limits in the R, I and J bands (optical). The excess in the near-IR is typically produced by a disk (Hulleman et. al. 2001, ApJ, 563, L49). The parameters of the black-body+disk spectrum are $R_{\rm WD} = 3.0 \times 20^8$ cm, $T = 7.0 \times 10^4$ K, $T_{\rm in} = 2.0 \times 10^3$ K and $R_{\rm out} = R_\odot$ (Boshkayev et. al. A&A 555:A151 (2013)).

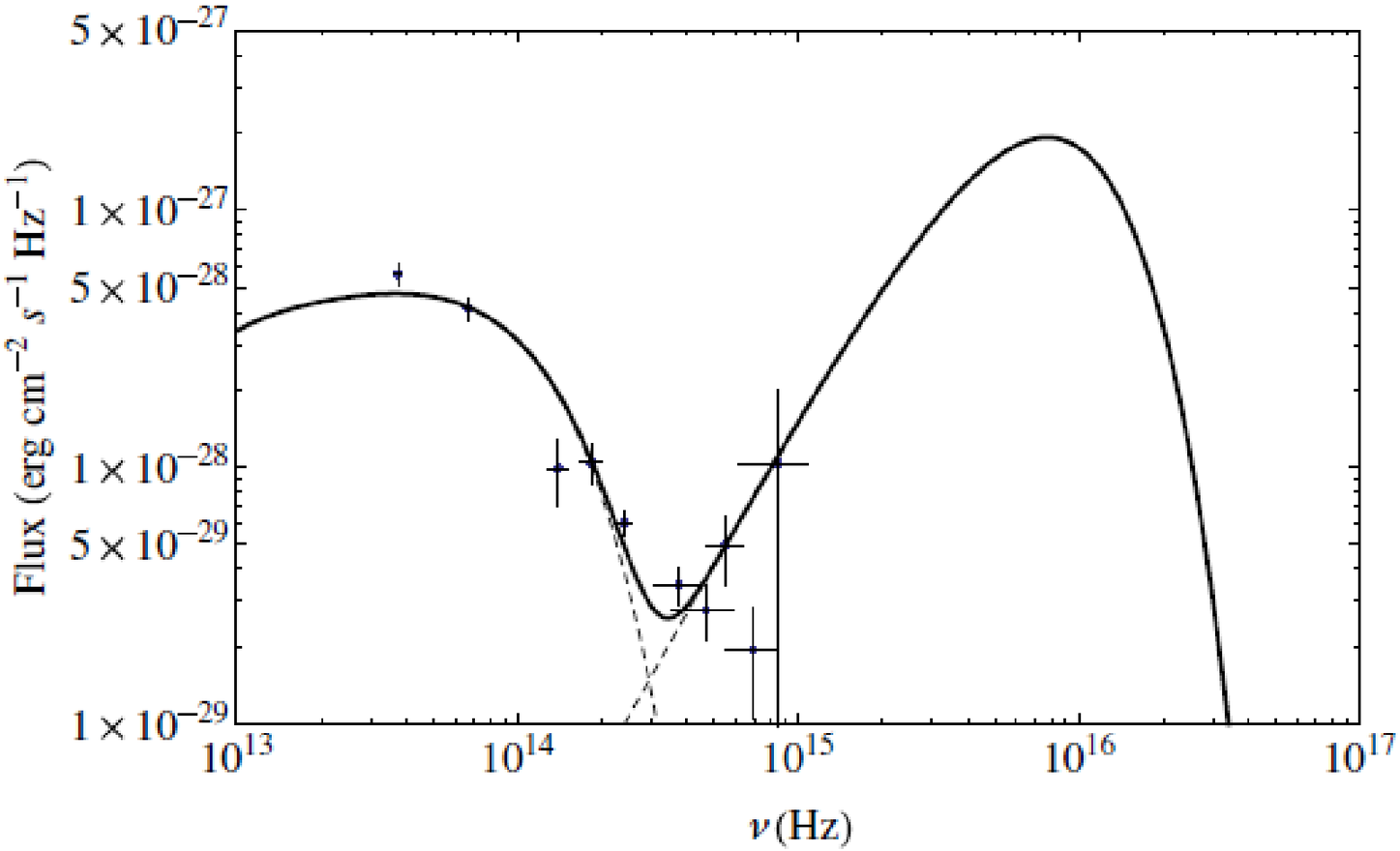

Figure 6. Observed and fitted spectrum of 4U 0142+61. The parameters of the black-body+disk spectrum (disk model of Chiang & Goldreich 1997) are $R_{\rm WD} \approx 0.006 R_\odot$, $T_{\rm eff} \approx 1.31 \times 10^5$ K, inner and outer disk radii $R_{\rm in} = 0.97 R_\odot$, $R_{\rm out} = 51.1 R_\odot$ and corresponding inner and outer disk temperatures $T_{\rm in} \approx 1950$ K and $T_{\rm out} \approx 100$ K, respectively. Taken from Rueda et. al., ApJL 772, L24 (2013).

4. Magnetosphere of rotationally powered pulsars

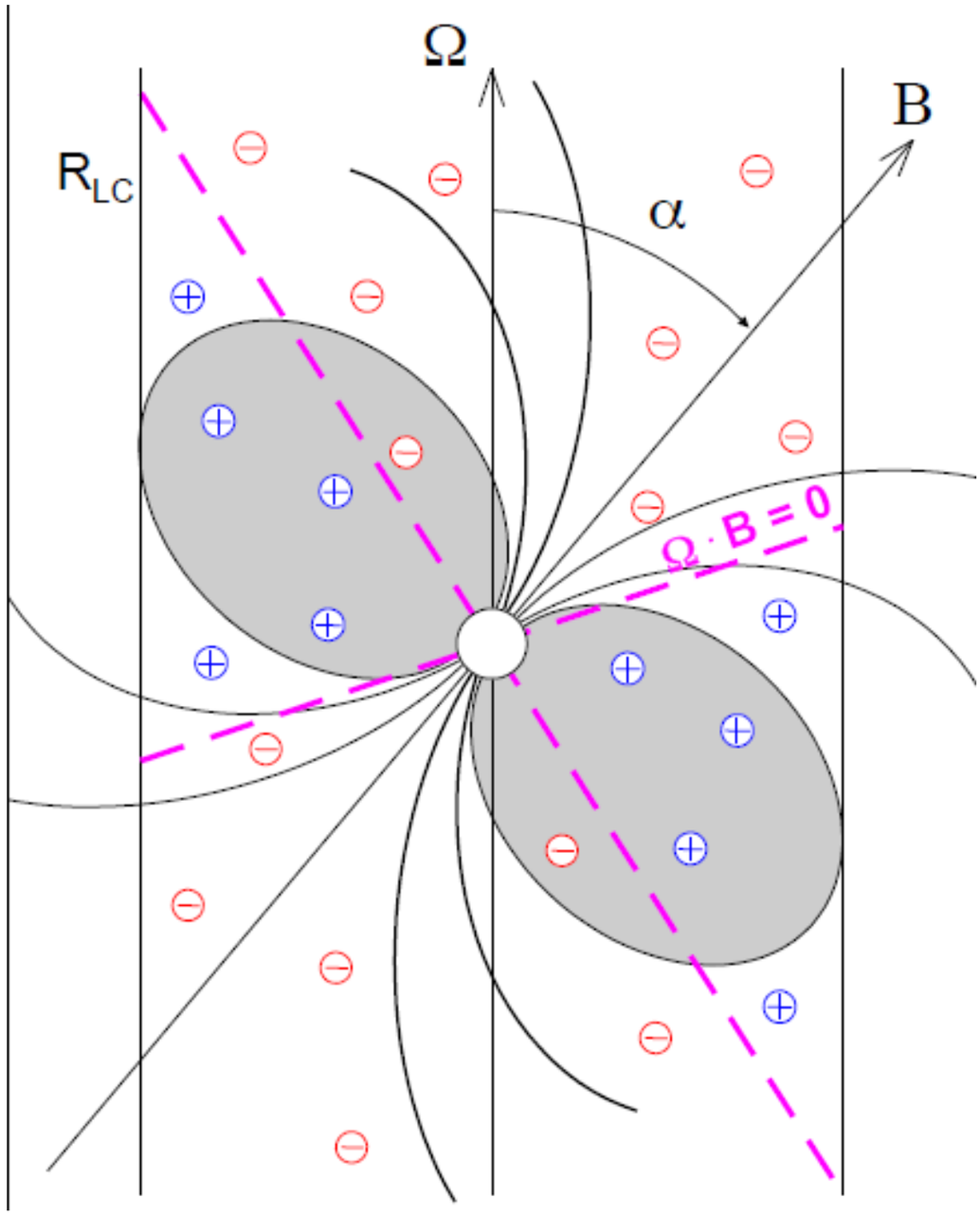

- The local density of charged plasma within the corotating magnetosphere is (Goldreich & Julian 1969)

$$\rho_{GJ} = -\frac{\Omega \cdot \mathbf{B}}{2\pi c} \frac{1}{1 - (\Omega r_{\perp}/c)^2}, \tag{5}$$

  where $r_{\perp} = r \sin\theta$ with θ the polar angle.

- The last B-field line closing within the corotating magnetosphere can be easily located from the B-field lines equation for a magnetic dipole $r/\sin^2\theta = \text{constant} = c/\Omega \equiv R_{\rm lc}$ and is located at an angle $\theta_{\rm pc} = \sqrt{2\pi R/(cP)}$ from the star's pole.

- The B-field lines that originate in the region between $\theta = 0$ and $\theta = \theta_{\rm pc}$ cross the light cylinder and are called *open field lines*. The size of the cap is given by the polar cap radius $R_{\rm pc} = R\theta_{\rm pc} \approx R\sqrt{2\pi R/(cP)}$.

Possible acceleration sites

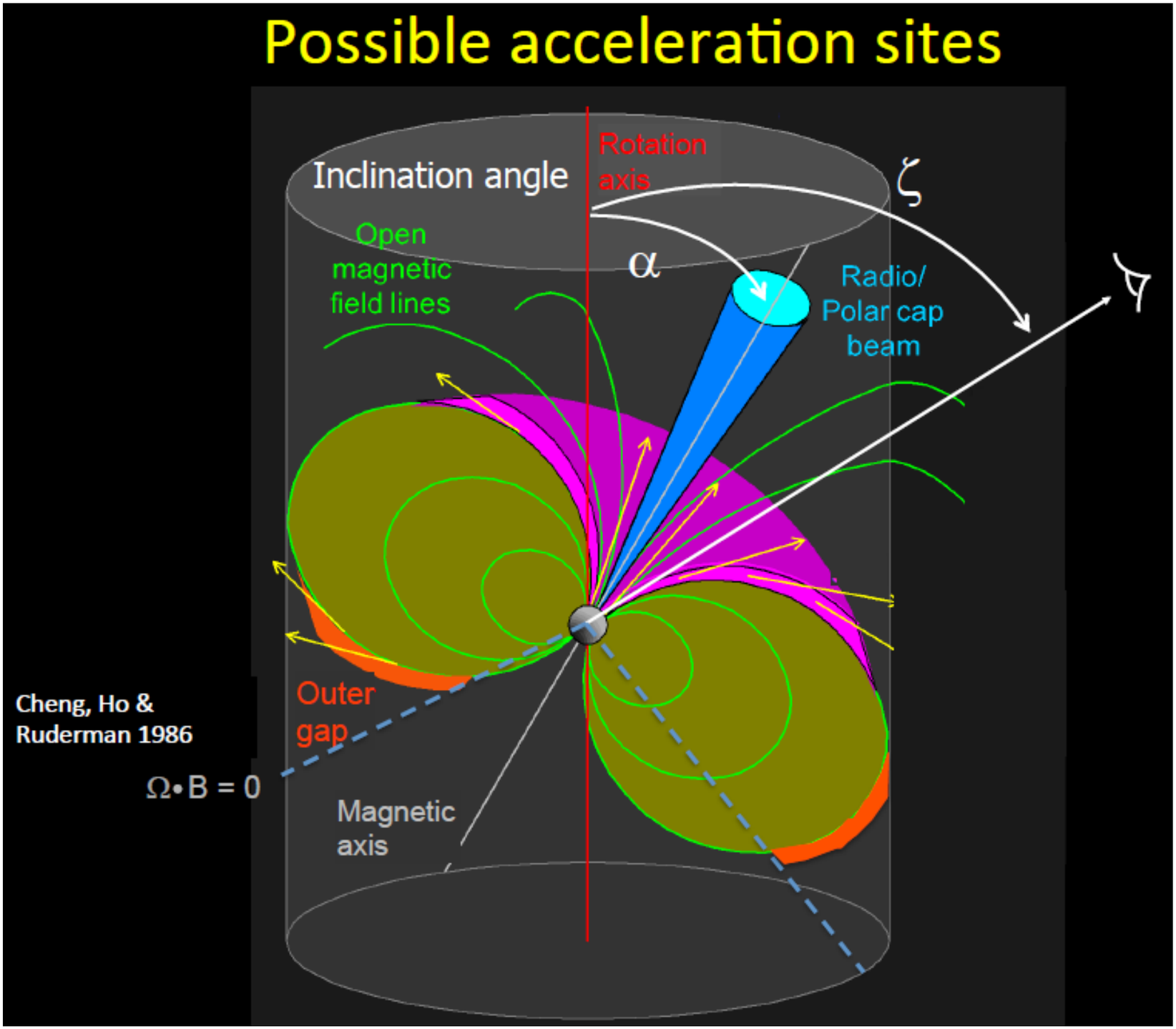

5. Polar Cap Model

5.1. Pulsar death-line or pair production threshold

To produce an avalanche of electron-positron pairs created by the interaction of the curvature gamma rays with a dipolar magnetic field, the WD must satisfy (Chen & Ruderman ApJ 402, 264 (1993), Kashiyama et. al. PRD. 83:023002 (2011):

$$B \geq \left(\frac{\sqrt{2\pi}}{240\pi^8}\right)^{1/4} \left(\frac{cP}{R}\right)^{15/8} \left(\frac{\lambda}{R}\right)^{1/2} B_{\rm c} \tag{6}$$

where $\lambda = \frac{\hbar}{mc}$ is the electron Compton wavelength and $B_{\rm c} \equiv \frac{m^2c^3}{e\hbar}$ is the quantum electrodynamic field, being m the electron mass, e the fundamental electric charge. c the speed of light and $\hbar$ the reduced Planck constant. For a multipolar case, this expression is modified by:

$$B > \left(\frac{\sqrt{2\pi}}{120\pi^7}\right)^{1/4} \left(\frac{cP}{R}\right)^{13/8} \left(\frac{\lambda}{R}\right) B_{\rm c} \tag{7}$$

5.2. Luminosity and temperature from bombardment of positrons

The surface temperature of the heated polar cap is (Cheng and Ruderman 1977):

$$(kT)^4 = 120\hbar^3 f^{-1} B^2 P^{-3} R^3, \tag{8}$$

where $f \leq 1$ is the fraction of the polar cap area filled by the spark discharge, $f \equiv R_{\rm bb}^2/R_{\rm pc}^2 \equiv c/2\pi R_{\rm bb}^2 R^{-3} P$. The radius $R_{\rm bb}$ is the black-body radius and $R_{\rm pc} := R\sqrt{\frac{2\pi}{c}RP}$ is the radius of the polar cap. We then have:

$$B = (kT)^2 (120\hbar^3)^{-1/2} \left(\frac{c}{2\pi}\right)^{1/2} R_{\rm bb} R^{-3} P^2. \tag{9}$$

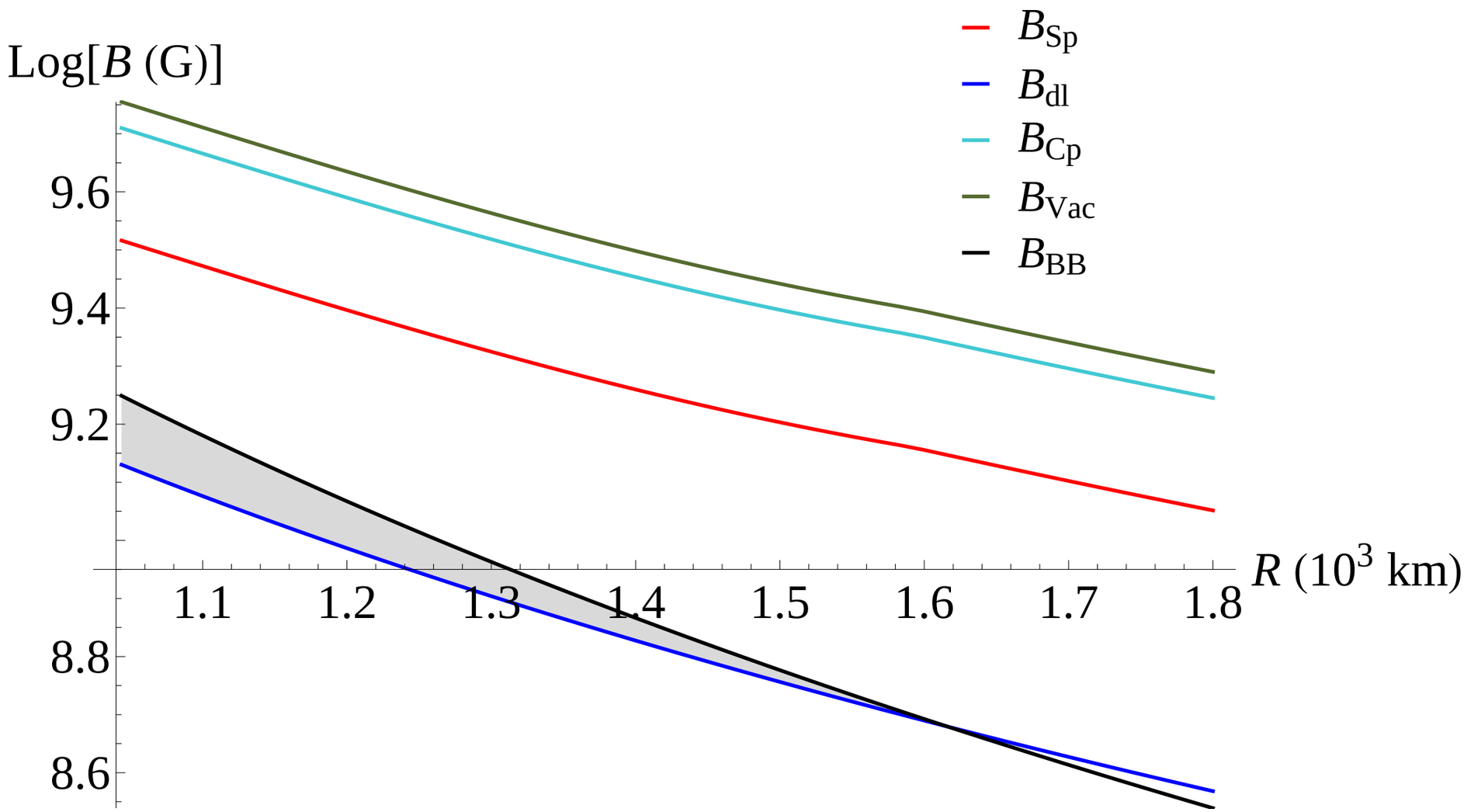

Figure 6. For 1E2259+5726, we see that for the vacuum, Contopoulos and Spitkovsky (90 degrees) cases, the magnetic field is above death-line. Here we assume a dipole magnetic field in the surface. However, the values coming from the polar cap, assuming validity of equation (8) are restricted.

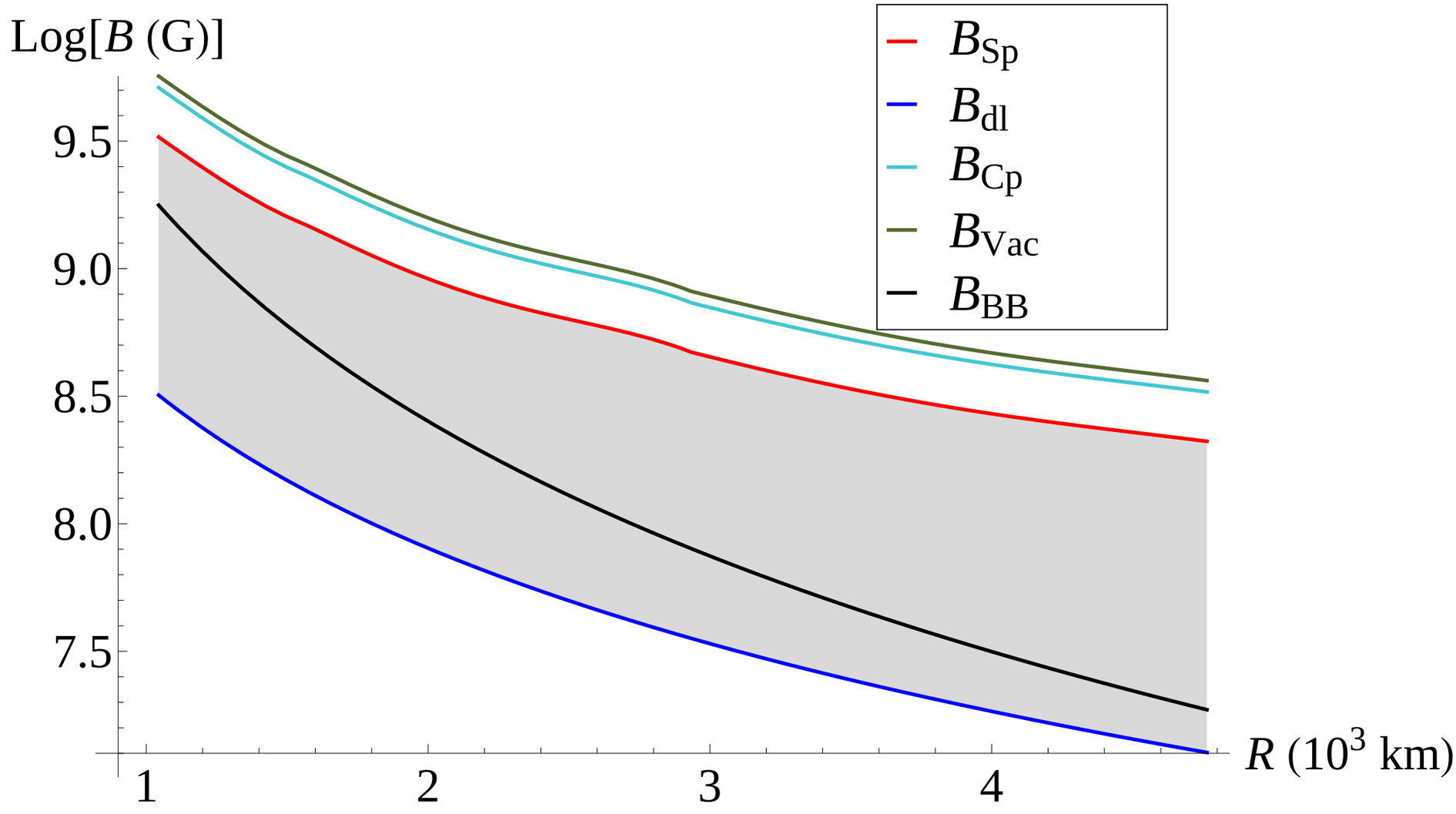

Figure 7. For 1E2259+5726, we see that for the vacuum, Contopoulos and Spitkovsky (90 degrees) cases, the magnetic field is above death-line. Here we assume a multipolar magnetic field in the surface. In this case, the range of possible values for the radius of the white dwarf is larger than in the dipolar case.

6. Outer gap model

- A fundamental parameter in this model is the *transfield fractional size of the gap* (also referred to as the gap size/thickness), f, defined as:

$$f \equiv \frac{\theta_{\rm c} - \theta_{\rm u}}{\theta_{\rm c}}, \tag{10}$$

- where $\theta_{\rm c}$ and $\theta_{\rm u}$ are the magnetic colatitudes of the footpoints on the PC surface for the lower and upper boundary, respectively.

- When $f = 1$ the outer gap embraces all open field lines.

$$f = \left(\frac{1}{3\pi}\right)^{7/6} \sqrt{ec}\, h_{\rm GeV\cdot\,s} (0.87)^{2/3}\, 10^{-16} (kT_{\rm keV})^{-2/3} R_8^{-3/2} B_8^{-1/2} P^{7/6} \tag{11}$$

$$f = 0.33 (kT_{\rm keV})^{-2/3} R_8^{-3/2} B_8^{-1/2} P^{7/6} \tag{12}$$

$$(kT)_{\rm th} = \left(\frac{60\hbar^3 c^2}{\pi^2 e}\right)^{1/4} (10.3)^{1/4} B^{1/4} P^{-1/6}. \tag{13}$$

$$A_{\rm OG} = 2\pi f \left(1 - \frac{f}{2}\right) \frac{2\pi R^3}{cP}. \tag{14}$$

$$A_{\rm eff} = A_{\rm OG} \left(\frac{(kT)_{\rm th}}{kT_{\rm obs}}\right)^4. \tag{15}$$

- For 4U 0142+61 $P = 8.69$ s, $kT = 0.41$ keV.

$R(10^8$ cm), $B(10^8$ G)	f	$A_{\rm eff}$ in $(10^{11}{\rm cm}^2)$
$R_{\rm max} = 5.4$, $B_{\rm min} = 6.3$	0.325	7.19
$R_{\rm min} = 1.05$, $B_{\rm max} = 1.3 \times 10^2$	1.38	

The measured area is 7.09×10^{11} cm^2.

- For SGR 0526-66 $P = 8.05$ s, $kT = 0.44$ keV.

$R(10^8$ cm), $B(10^8$ G)	f	$A_{\rm eff}$ in $(10^{11}{\rm cm}^2)$
$R_{\rm max} = 5.17$, $B_{\rm min} = 14.4$	0.23	9.23
$R_{\rm min} = 1.046$, $B_{\rm max} = 2.69 \times 10^2$	0.95	3.5

The measured area is 9.5×10^{11} cm^2.

- For SGR 1806-20 $P = 7.55$ s, $kT = 0.55$ keV.

$R(10^8$ cm), $B(10^8$ G)	f	$A_{\rm eff}$ in $(10^{11}{\rm cm}^2)$
$R_{\rm max} = 4.98$, $B_{\rm min} = 54.7$	0.12	8.2
$R_{\rm min} = 1.045$, $B_{\rm max} = 9.43 \times 10^2$	0.5	4.2

The measured area is 4.3×10^{11} cm^2.

- For 1E 2259+586 $P = 6.98$ s, $kT = 0.37$ keV.

$R(10^8$ cm), $B(10^8$ G)	f	$A_{\rm eff}$ in $(10^{11}{\rm cm}^2)$
$R_{\rm max} = 4.76$, $B_{\rm min} = 3.44$	0.39	7.1
$R_{\rm min} = 1.044$, $B_{\rm max} = 56.9$	1.5	

  The measured area is 5.8×10^{11} cm^2.

- For SGR 0418+5729 $P = 9.08$ s, $kT = 0.32$ keV.

$R(10^8$ cm), $B(10^8$ G)	f	$A_{\rm eff}$ in $(10^{11}{\rm cm}^2)$
$R_{\rm max} = 5.5.12$, $B_{\rm min} = 0.27$	1.12	
$R_{\rm min} = 1.05$, $B_{\rm max} = 5.8$	4.8	

  In both cases we cannot have an outer gap because $f > 1$, which is a criteria to establish a death-line.

7. Conclusions

- The effect of the wind, as shown in the works of Spitkovsky 2006 and Contopoulos et. al. 2014, reduces the value of B with respect to its value in the vacuum case.

- Compatibility in the optical band was already verified in Boshkayev et. al. A&A 555:A151 (2013) and Rueda et. al., ApJL 772, L24 (2013), and here we have verified the thermal X-ray emission. Both analysis give a value of the radius compatible with the WD and inside the range of stability stablished for a WD.

- It was shown that 1E2259+5726 described as a WD was in the range of stability and above the threshold of pair production in the polar cap model. The same for other sources not shown in this presentation.

- The thickness factor f puts further constraints to the range of radii and masses, in some cases showing it is not possible to have an outer gap, as shown, for example, for the SGR0418+5729 source.